Osborn, M. J., Gander, J. E., Parisi, E., & Carson, J. (1972) *J. Biol. Chem. 247*, 3962-3972.
Otto, H., Marti, T., Holz, M., Mogi, T., Lindau, M., Khorana, H., & Heyn, M. (1989) *Proc. Natl. Acad. Sci. U.S.A. 86*, 9228-9232.
Otto, H., Marti, T., Holz, M., Mogi, T., Stern, L., Engel, F., Khorana, H., & Heyn, M. (1990) *Proc. Natl. Acad. Sci. U.S.A. 87*, 1018-1022.
Pfeifer, F., Weidinger, G., & Goebel, W. (1981) *J. Bacteriol. 145*, 375-381.
Sanger, F., Nicklen, S., & Coulson, A. R. (1977) *Proc. Natl. Acad. Sci. U.S.A. 74*, 5463-5467.
Shepard, H., Yelverton, E., & Goeddel, D. (1982) *DNA 1*, 125-131.
Soppa, J., & Oesterhelt, D. (1989) *J. Biol. Chem. 264*, 13043-13048.
Soppa, J., Otomo, J., Straub, J., Tittor, J., Meessen, S., & Oesterhelt, D. (1989) *J. Biol. Chem. 264*, 13049-13056.
Stoeckenius, W., & Bogomolni, R. A. (1982) *Annu. Rev. Biochem. 52*, 587-616.
Towbin, H., Staehelin, T., & Gordon, J. (1979) *Proc. Natl. Acad. Sci. U.S.A. 76*, 4350-4354.
Tsang, V. C. W., Peralta, J. M., & Simons, A. R. (1983) *Methods Enzymol. 92*, 377-391.
Wolfer, U., Dencher, N. A., Buldt, G., & Wrede, P. (1988) *Eur. J. Biochem. 174*, 51-57.
Yanisch-Perron, C., Vieira, J., & Messing, J. (1985) *Gene 33*, 103-119.
Zabin, I., & Fowler, A. V. (1978) in *The Operon* (Miller, J. H., & Reznikoff, W. S., Eds.) pp 89-121, Cold Spring Harbor Laboratory, Cold Spring Harbor, NY.

Wild-Type and Mutant Bacteriorhodopsins D85N, D96N, and R82Q: Purification to Homogeneity, pH Dependence of Pumping, and Electron Diffraction†

Larry J. W. Miercke, Mary C. Betlach, Alok K. Mitra, Richard F. Shand,‡ Susan K. Fong, and Robert M. Stroud*
Department of Biochemistry and Biophysics, University of California, San Francisco, San Francisco, California 94143-0448
Received August 14, 1990; Revised Manuscript Received November 26, 1990

ABSTRACT: Bacterioopsin, expressed in *Escherichia coli* as a fusion protein with 13 heterologous residues at the amino terminus, has been purified in the presence of detergents and retinylated to give bacteriorhodopsin. Further purification yielded pure bacteriorhodopsin, which had an absorbance ratio ($A_{280}/A_{\lambda_{max}}$) of 1.5 in the dark-adapted state in a single-detergent environment. This protein has a folding rate, absorbance spectrum, and light-induced proton pumping activity identical with those of bacteriorhodopsin purified from *Halobacterium halobium*. Protein expressed from the mutants D85N, D96N, and R82Q and purified similarly yielded pure protein with absorbance ratios of 1.5. Proton pumping rates of bacteriorhodopsins with the wild-type sequence and variants D85N, D96N, and R82Q were determined in phospholipid vesicles as a function of pH. D85N was inactive at all pH values, whereas D96N was inactive from pH 7.0 to pH 8.0, where wild type is most active, but had some activity at low pH. R82Q showed diminished proton pumping with the same pH dependence as for wild type. Bacteriorhodopsin purified from *E. coli* crystallized in two types of two-dimensional crystal lattices suitable for low-dose electron diffraction, which permit detailed analysis of structural differences in site-directed variants. One lattice was trigonal, as in purple membrane, and showed a high-resolution electron diffraction pattern from glucose-sustained patches. The other lattice was previously uncharacterized with unit cell dimensions a = 127 Å, b = 67 Å, and symmetry of the orthorhombic plane group *pgg*.

Structural analysis of proteins by crystallography, by infrared or Raman spectroscopy, requires large, many milligram quantities of pure protein. In the preceding paper, we describe an efficient expression system for bacteriorhodopsin (BR)[1] in *Escherichia coli* (Shand et al., 1991). To improve the chances of obtaining high-resolution diffraction from two- and three-dimensional crystals of BR and site-directed variants of BR, we developed a purification scheme which yields homogeneous ~100% pure BR and proteins made from site-directed mutants of BR in a single-detergent system. Our method differs from the organic extraction procedure of Braiman et al. (1987), which produces ~80% pure BR in a complex mixed-micelle system.

†Supported by National Institutes of Health Grants GM32079 to R.M.S. and GM31785 to M.C.B. and by National Research Service Award 5T32CA09043 to R.F.S.
*Author to whom correspondence should be addressed.
‡Present address: Department of Biological Sciences, Northern Arizona University, Flagstaff, AZ 86011.

[1] Abbreviations: BR, bacteriorhodopsin; BO, bacterioopsin; PM, purple membrane; w-BO, bacterioospin purified from *Halobacterium halobium*; w-BR, w-BO complexed with retinal; e-BO, bacterioopsin expressed from pβgbop in *E. coli*; e-BR, e-BO complexed with retinal; d-BR, delipidated BR; HR, halorhodopsin; NG, nonyl glucoside; OG, octyl glucoside; SDS, sodium dodecyl sulfate; CHAPSO, 3-[(cholamidopropyl)dimethylammonio]-2-hydroxyl-1-propanesulfonic acid; CHAPS, 3-[(cholamidopropyl)dimethylammonio]-1-propanesulfonate; SDS-PAGE, SDS-polyacrylamide gel electrophoresis; βME, β-mercaptoethanol; HPSEC, high-performance size-exclusion chromatography; DMPC, dimyristoylphosphatidylcholine; ADA, *N*-(2-acetamido)iminodiacetic acid; TX-100, Triton X-100; CMC, critical micellar concentration; LA, light adapted; DA, dark adapted; A_λ, absorbance at wavelength λ;

0006-2960/91/0430-3088$02.50/0

Site-directed mutagenesis has identified residues whose protonation state changes during the photocycle, and residues whose substitution affects the chromophore environment (Khorana, 1988). To help establish the role of altered residues in the photoreaction cycle, it is necessary to characterize any changes in structure in addition to function. The three-dimensional structure of bacteriorhodopsin has been determined from electron imaging to a resolution of about 3.5-Å in-plane by ~10-Å perpendicular to the membrane plane (Henderson et al., 1990). With the resulting phases, any changes in structure could now be characterized in three dimensions by comparing electron diffraction amplitudes alone, using difference Fourier methods. Initially, the degree of structure change can readily be quantitated in projection onto the membrane plane by using electron diffraction intensities in projection (Hayward & Glaeser, 1980) which we have recorded to 2.65-Å resolution from native PM patches (Hayward & Stroud, 1981), or which can be recorded from larger reconstituted patches (Henderson et al., 1986) that are twinned crystals. Intensities from the twinned components can be extracted by refining the degree of twinning (Mitra & Stroud, 1990; Henderson et al., 1990). By use of changes in the in-plane diffraction intensities along with phases determined from image reconstruction of electron micrographic images (Hayward & Stroud, 1981; Baldwin et al., 1988), changes in density of as little as two to three carbon atoms are identifiable by Fourier difference mapping in projection (Mitra & Stroud, 1990).

BR is a light-driven proton pump that is 32% identical in sequence with a light-driven chloride pump, HR (Blanck & Oesterhelt, 1987; Oesterhelt & Tittor, 1989). The chromophore *all-trans*-retinal is attached to Lys-216 by a protonated Schiff base in BR (Katre et al., 1981; Bayley et al., 1981; Rothschild et al., 1982) and to an analogous lysine residue in HR (Smith et al., 1984; Alshuth et al., 1985). In BR, absorption of light leads very rapidly to isomerization of retinal about the C_{13}=C_{14} bond (Mathies et al., 1988). This initiates a photoreaction cycle in which several intermediates are recognized and characterized by their wavelength of maximum absorbance as $BR_{568} \rightarrow J_{625} \rightarrow K_{610} \rightarrow L_{550} \rightarrow M_{412} \rightarrow N_{550} \rightarrow O_{640} \rightarrow BR_{568}$ (Lozier et al., 1975; Kouyama et al., 1988; Hofrichter et al., 1989). In BR, deprotonation of the Schiff base occurs in the $L_{550} \rightarrow M_{412}$ transition (Lozier et al., 1976). Analysis of site-directed mutations has identified Asp-85 as the residue to which the Schiff base proton is directed upon isomerization (Braiman et al., 1988; Gerwert et al., 1989) and Asp-96 as a residue of raised pK_a which provides the proton for reprotonation of the Schiff base from the cytoplasmic side of the chromophore. Reprotonation of the Schiff base occurs during the $M_{412} \rightarrow N_{550}$ transition (Fodor et al., 1988) and is followed by reisomerization back to *all-trans*-retinal in the $N_{550} \rightarrow O_{640}$ transition (Smith et al., 1983) and reprotonation of the protein (Ames & Mathies, 1990).

The long axial direction of retinal is oriented at 23° to the membrane plane and lies between the center of the bilayer and the outside of the cell membrane (Heyn et al., 1977; Earnest et al., 1986; Lin & Mathies, 1989). Asp-85 and Asp-96, 11 residues apart in sequence, are separated by about 15.5 Å as they lie in transmembrane α-helix C, and on opposite sides of the Schiff base (Lin & Mathies, 1989; Henderson et al., 1990). This distance is too great for both to be in contact with the Schiff base nitrogen on Lys-216, even allowing for its reorientation during photoisomerization. Asp-212, one helical turn from Lys-216 on helix G, also has a significant effect on the charge environment around the Schiff base (Braiman et al., 1988; Gerwert et al., 1989). Thus, in BR_{568}, the charges on Asp-85 and Asp-212, and probably Arg-82, interact with each other and with the Schiff base. Alterations of these titratable groups affect proton pumping, the wavelength of maximal absorbance, and photocycle kinetics. Since the pH dependence of pumping may reflect the pK_a's of groups involved in the photoreaction cycle, we recorded proton pumping rates versus pH for D85N, D96N, and R82Q. The changes in structure due to these substitutions will be described subsequently.

Materials and Methods

Buffers. Buffers used were the following: 50 mM sodium phosphate, pH 7.2 (buffer A); 18 mM NG (Cal Biochem, San Diego, CA)/5 mM sodium acetate, pH 5.0 (buffer B); 100 mM sodium acetate/4 mM sodium azide, pH 5.0 (buffer C); 10 mM sodium acetate/4 mM sodium azide, pH 5.0 (buffer D); 0.1% (w/v) SDS (Bio-Rad, Richmond, CA)/100 mM sodium acetate, pH 6.0 (buffer E); 16.4 mM CHAPSO (Boehringer Mannheim Biochemicals, Indianapolis, IN), 100 mM sodium chloride, and 20 mM sodium acetate, pH 5.0 (buffer F); 1 mM ADA, pH 6.5 (buffer G). All buffers were sterilized by passage through a 0.2-μm pore-size filter (Millipore Corp., Bedford, MA).

Expression and Quantitation of BO and BR. Expression of BO in *E. coli* and site-directed mutagenesis were as described (Shand et al., 1991). Quantitation of BR, total protein, protein concentration, SDS–PAGE, and Western blot analysis were performed as described by Miercke et al. (1989a), except that a Shimadzu UV-160 spectrophotometer was used for absorption spectroscopy, a least-squares analysis of the log of the optical density versus the log of protein concentration was used for quantitating total protein, and YM-30 high-pressure filtration membranes (Amicon, Beverly, MA) were used for concentrating protein solutions. Comparison between the DA visible absorbance and total protein determined by the colorimetric Lowry assay (Lowry et al., 1951) was used to assess BR purity. Throughout the purification, BO was monitored by Western blot analysis (see Figure 2B) and quantitated spectrophotometrically after generation of BR by retinal addition.

Purification of e-BO. Procedures prior to membrane solubilization were carried out at 4 °C while membrane solubilization and column chromatography were performed at room temperature. Cells containing e-BO were grown as described (Shand et al., 1991), harvested, resuspended at 2 mL/g of cells (wet weight) in buffer A containing 2 μg each of DNase I and RNase A per milliliter, and then lysed by two passes through a French pressure cell. The lysate was diluted with 3 volumes of buffer A, stirred for 30 min, and centrifuged for 3 h at 143000*g*. The crude membranes were washed in buffer A containing 4.5 M urea and 2 M NaCl for 2 h followed by washing for 30 min in buffer A titrated to pH 10.5. Washed membranes were solubilized in buffer A containing 2% (w/v) SDS for 15 min with stirring, boiled for 1 min, and centrifuged for 1.5 h at 143000*g*. The supernatant was brought to 4% (v/v) βME, boiled for 1 min, and filtered through a 0.4-μm Nalgene disposable filter (Sybron Corp., Rochester, NY).

e-BO was purified from the filtered, SDS-solubilized membranes by HPSEC using two TSK G3000SW columns: 5 cm × 60 cm and 2.2 cm × 60 cm (Bio-Rad, Richmond, CA). The columns were run in buffer E (SDS mobile phase) with flow rates of 10 and 2 mL/min, respectively. Fractions containing e-BO were pooled and concentrated between column applications. e-BO fractions from the final column with an A_{280}

greater than 1.5 were pooled for incorporation of retinal.

Retinylation of e-BO. Conditions for generating e-BR from e-BO were as described by Braiman et al. (1987), with the following modifications. The reaction mixture contained 33 mM sodium acetate at pH 6.0, 0.03% (w/v) SDS, 0.25% (w/v) DMPC (Avanti Polar Lipids, Inc., Birmingham, AL), 0.25% (w/v) CHAPSO, ~0.6 mg/mL e-BO, and 2 molar equiv (retinal to protein) of *all-trans*-retinal (Sigma Chemical Co., St. Louis, MO; prepared as a concentrated stock in ethanol with final ethanol concentration <0.5% v/v). For e-BO variants containing single amino acid substitutions, concentrations of DMPC and CHAPSO of 0.5% (w/v) were used for maximum retinylation. After 10–15 h of incubation, SDS, DMPC, excess CHAPSO, and excess retinal were removed by HPSEC using buffer F (CHAPSO mobile phase) as described previously (Miercke et al., 1989b). Prior to column injection, the reaction mixture was filtered through a 0.2-μm Acrodisk (Gelman Sciences, Ann Arbor, MI) and concentrated to ~3 mL.

Detergent Exchange and Removal of Unretinylated BO. CHAPSO-containing samples were exchanged with NG by filtration using a 12-mL stirred cell and a YM-30 membrane. Typically, 7 mg of protein in 1 mL of buffer F was brought to 10 mL with buffer B and then concentrated to 2 mL. Three cycles of detergent exchange were followed by dye–ligand affinity chromatography to remove unretinylated BO from BR. A 1 cm × 3 cm column of "Red A" (Amicon, Beverly, MA) was prepared according to manufacturer's specifications and equilibrated with buffer B at 4 °C. Following sample application, the matrix was washed with 5 bed volumes of buffer B. The protein was eluted in buffer B containing 0.5 mM NaCl.

Isolation of w-BR from H. halobium. w-BO in SDS and w-BR in CHAPSO and NG were prepared from PM (provided by Walter Stoeckenius) as described for e-BO and e-BR except for the following: (i) the buffer, urea/NaCl, and alkaline membrane washes were omitted; (ii) βME was not added to SDS-solubilized PM (5 mg of BR/mL); and (iii) the largest size exclusion column (5 cm × 60 cm) was omitted. d-BR was prepared from PM by solubilizing in TX-100 (Pierce, Rockford, IL) and delipidated by using HPSEC run in CHAPSO (Miercke et al., 1989b).

Proton Pumping Assays. BR activity was determined by quantitating light-induced proton pumping as described previously (Miercke et al., 1989b) following incorporation of BR into soybean phospholipid vesicles by detergent dialysis. BR/CHAPSO was mixed with lipid/CHAPSO, and vesicles were prepared by dialysis against buffer G containing 0.15 M NaCl and 0.15 M KCl. Vesicles were diluted in dialysis buffer to 0.35 nM BR, valinomycin was added to 0.2 μM, and the pH was adjusted by slow titration with either 0.1 M NaOH or 0.1 M HCl. Functional parameters (initial rate, steady state, and initial decay) were corrected for light-dependent electrode effects and for orientation of BR molecules in the vesicles. The orientation in vesicles was determined by chymotryptic cleavage and found to be ~31% ± 4% pumping outward, implying ~69% ± 4% pumping inward (Miercke et al., 1989b). BR was quantitated spectrophotometrically after vesicle solubilization in TX-100.

Crystallization of e-BR into Two-Dimensional Lattices and Electron Microscopy. CHAPSO was exchanged for TX-100 at 4 °C in a stirred filtration cell with at least six repetitions using TX-100 in buffer C at a 6:1 (w/w) detergent to protein ratio. Protein concentration was typically 6 mg/mL in 3% (w/v) TX-100. Following detergent exchange, CHAPSO concentration was calculated to be <0.1 mM, based on the rate of CHAPSO removal as determined by thin-layer chromatography. Polar lipids extracted either from PM or from whole cells of *H. halobium* (Kates et al., 1982) were solubilized in buffer C containing 2% TX-100 (v/v). These lipids were added to e-BR/TX-100 in a lipid to protein ratio of 1:3 (w/w) and incubated with stirring in the dark at 4 °C for 12–24 h. The protein was concentrated in a Centricon-10 (Amicon, Beverly, MA) to 10–15 mg/mL and centrifuged at 80000*g* for 1 h to remove insoluble particulates. TX-100 was removed by dialysis (Spectropore 6; 25 000 molecular weight cutoff) against buffer C for 2–4 weeks in the dark at 4 °C. Dialysis was deemed complete when the sample, pelleted for 45 min at 40000*g*, yielded a visibly clear supernatant. e-BR reconstituted into *H. halobium* lipids was resuspended in buffer D, stored in the dark at 4 °C, and periodically inspected for crystalline specimens in a Phillips EM400 electron microscope (Phillips Electronic Instruments, Eindhoven, The Netherlands).

Electron images were recorded under low-dose conditions. A 5-μL sample was applied to a parlodian-coated 400-mesh copper grid, overlaid with a carbon film that was rendered hydrophilic by glow discharge in air. The sample was allowed to settle for 2 min, partially blotted, and stained with uranyl formate, prepared according to Williams (1981) for 30 s. Finally the grid was reblotted and air-dried. For electron diffraction, 400-mesh copper grids were covered by a thin carbon film floated away from freshly cleaved mica. Prior to sample application, the grid was coated with 1% (w/v) ovalbumin (Sigma) for 1 min and blotted. Next, 5-μL samples were applied, allowed to stand for 2 min, and then partially blotted. Five microliters of 0.7% (w/v) glucose in aqueous solution was applied for 1 min and wicked away with filter paper, and the grid was air-dried. Electron diffraction was carried out initially on samples at room temperature as described by Mitra and Stroud (1990), at 100-kV accelerating voltage using a 50-μm diameter condenser aperture, 0.2-μm spot size, and a total dose of ~0.5 e/Å^2.

Results

Purification of e-BO. Sequential washing of the *E. coli* membranes with buffer, urea/NaCl, and buffer at pH 10.5 removed approximately 70% of total non-BO proteins as determined by the Lowry method, to give the material shown in Figure 2, lane 3. Of the remaining membrane proteins, including e-BO, 90–100% was solubilized in 2% SDS at pH 7.2 and subjected to HPSEC. e-BO eluted in a region of the profile which was devoid of significant amounts of other proteins and is clearly visible as the second largest peak in a HPSEC profile of protein from induced cells (Figure 1A, inset, lower trace). e-BO enrichment from successive column chromatography runs is indicated in Figure 1A–C. Final protein composition is shown in Figure 2A, lane 4. The three bands seen were identified as e-BO (Figure 2B, lane 4). Excess SDS, lipid (and retinal in the case of PM) migrated in the peak trailing e-BO (Figure 1) as determined by separate injections of 2% SDS and radioactively labeled *H. halobium* lipids, and by photometric determination of the absorption spectrum for retinal. Multiple passes through HPSEC in SDS running buffer permit concentration of e-BO alongside purification. This yielded a final concentration of e-BR greater than 0.5 mg of BR/mL after retinylation.

Properties of e-BR and w-BR Are Essentially Indistinguishable. e-BR was generated by retinylation of e-BO. HPSEC in buffer F removed SDS, DMPC, excess retinal, and excess CHAPSO. Low amounts of SDS (0.03%) present during BO to BR retinylation ensured that BR was not de-

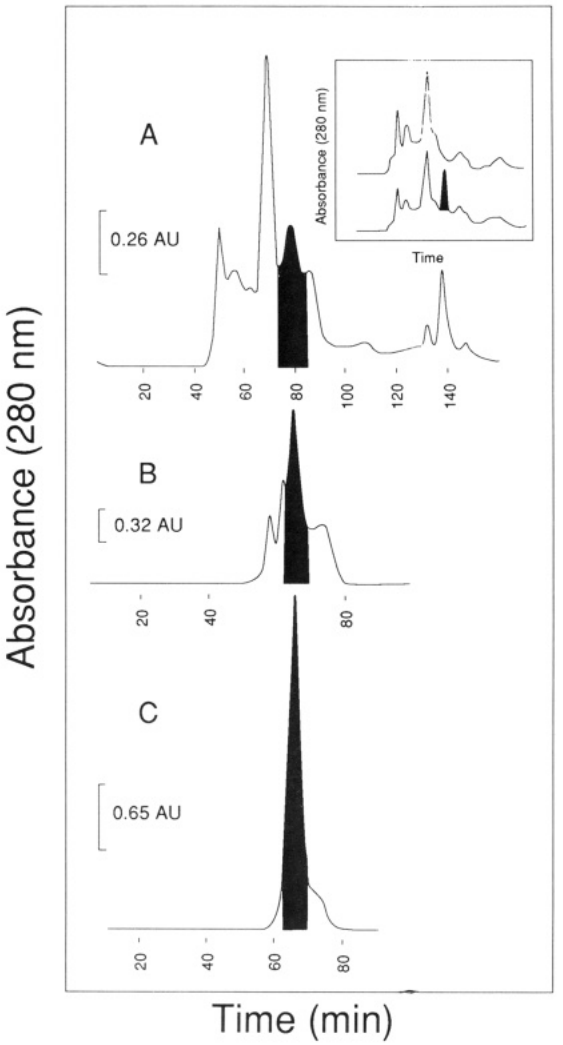

FIGURE 1: Profiles of A_{280} versus retention time from HPSEC steps summarizing e-BO purification, using an SDS mobile phase. Shaded regions indicate pooled fractions containing e-BO. (A) Profile showing A_{280} versus retention time for a large-scale preparation of SDS-solubilized washed membranes, run on HPSEC (TSK 5 × 60 cm). Inset: profile of HPSEC (TSK 2.2 × 60 cm column) performed on washed *E. coli* membrane proteins solubilized in SDS, from a 1-L preparation of uninduced (upper trace) and induced (lower trace) cells. Marked overproduction of e-BO is seen in the shaded peak. (B) Profile of pooled fractions from (A), subjected to HPSEC (TSK 2.2 × 60 cm). (C) Profile of pooled fractions from (B), subjected to HPSEC (TSK 2.2 × 60 cm).

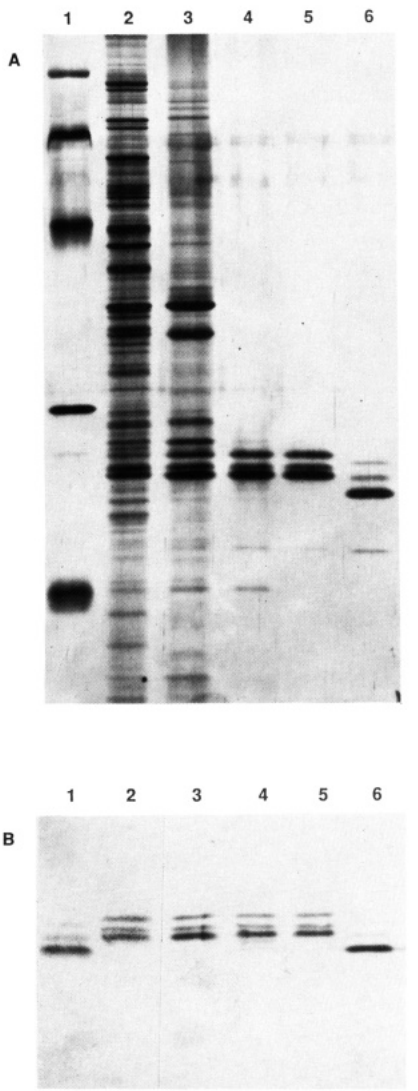

FIGURE 2: SDS–PAGE of e-BO samples during the purification procedure: (A) silver stained; (B) stained with antibodies against BR. Lanes 1: (A) molecular weight standards; (B) PM. Lanes 2: Initial lysate following French press treatment of cells. Lanes 3: The membrane fraction after washing. Lanes 4: e-BO following HPSEC in the SDS mobile phase and prior to BR generation. Lanes 5: e-BR following removal of unretinylated e-BO. Lanes 6: w-BR. The three bands seen for w-BR correspond to differential cleavage at the N-terminal end; the cleavage sites in w-BR are different than the cleavage sites in e-BO (Shand et al., 1991).

natured upon concentration by pressure filtration, as required for application to HPSEC in CHAPSO. If the SDS concentration is higher, more lipid and CHAPSO are required for maximum retinylation. Samples applied to HPSEC in CHAPSO that contain excessive lipid result in a broader peak for e-BO and incomplete delipidation, and therefore yield less usable material.

e-BR was purified to homogeneity as verified by identical silver and antibody staining patterns (Figure 2A,B, lane 5). The yield of e-BR from SDS-solubilized washed membranes (Figure 2, lane 3) to the final product (Figure 2, lane 5) was 60%. The folding rates upon retinylation were identical for e-BO and w-BO, characterized by a $t_{1/2}$ (time to reach 50% BR generation) of 1.3 min (Table I). BR generation was essentially complete within 20 min. Both w- and e-BR had absorption maxima of 556 nm. e-BR and w-BR exhibited similar HPSEC/CHAPSO profiles, contain greater than 95% BR at this stage, and have identical UV–visible absorption properties in CHAPSO as for delipidated BR monomers which had not been denatured and renatured (Miercke et al., 1989b). Upon light adaptation, the dark-adapted absorption maximum of 548 nm ($A_{280nm}/A_{\lambda_{max}} = 1.5$) underwent a red-shift to 556 nm with a 6–8% change in extinction coefficient (Figure 3, top panel).

Table I: Folding Properties[a] of e-BO from Wild Type and Mutants

e-BO/ mutant	$t_{1/2}$ (min)	total time (min)[b]	absorption maximum (nm)
e-BO	1.3	20	556
D96N	2.1	35	558
R82Q	4.6	70	583
D85N	170	900	594

[a] Folding conditions were 31 mM sodium acetate, pH 6.0, 0.03% SDS, 0.5% DMPC, 0.5% CHAPSO, and 2 equiv of *all-trans*-retinal. [b] Total time used to achieve optimal BR generation.

Due to incomplete retinylation of e-BO variants, and minimal discrimination or removal of BO by HPSEC/CHAPSO, a dye–ligand affinity chromatography step was used to separate BR from BO. This affinity step yielded greater than 90%

Table II: Summary of Purification and Properties of e-BR and Mutant Monomers

species	$A_{\lambda_{max}}$(DA) (nm)		$A_{280nm}/A_{\lambda_{max}}$ [c]		BR purity (%)[d]		yield (mg)	
	CHAPSO[a]	NG[b]	CHAPSO	NG	CHAPSO	NG	CHAPSO	NG
e-BR	548	548	1.5	1.5	97	100	14	13
D96N	550	556	1.8	1.5	93	100	14	13
R82Q	559	585	1.9	1.5	80	100	11	10
D85N	583	596	2.1	1.5	65	100	7	6

[a] Properties of material in 16 mM CHAPSO, pH 5. [b] Properties after the affinity step in 18 mM NG, pH 5. [c] The ratio $A_{280nm}/A_{\lambda_{max}}$ is described as the optical purity. [d] Comparison of the colorimetric Lowry assay and the DA visible optical density.

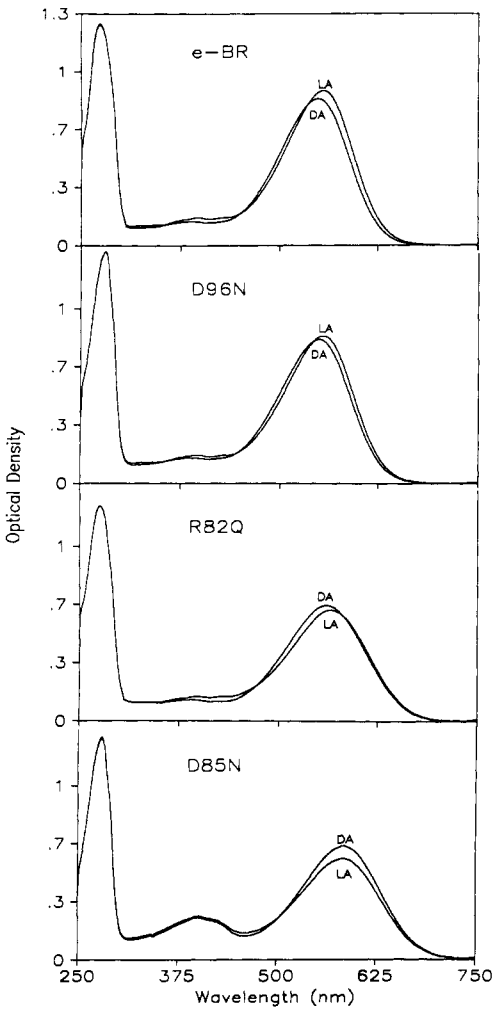

FIGURE 3: Absorption spectra of LA and DA monomeric e-BR and variants in CHAPSO, pH 5.0, following purification. Absorption properties are tabulated in Table II.

of the applied protein based on visible optical density and provides for detergent exchange into NG, a detergent in which BR exhibits the least perturbed photocycle when compared to PM (Milder et al., 1991). The purity of e-BR and variants was then ~100%, judged by the ratio of colorimetric Lowry assay to visible optical density (Table II).

The 3 species of e-BO revealed in the electrophoretic banding pattern (Figure 2, lane 5) are due to processing of 0, 1, and 4 residues from the 13 additional heterologous residues at the amino terminus of e-BO (Shand et al., 1991). Each band was excised from a polyacrylamide gel and electroeluted, and BR was generated (folded) separately (data not shown). Identical folding kinetics (7% standard deviation) and absorption maxima relative to mature w-BR were obtained for each purified e-BO polypeptide, indicating that these additional residues have no effect on e-BO to e-BR folding.

Purification and Characterization of e-BRs Containing Single Amino Acid Substitutions. Starting from equal

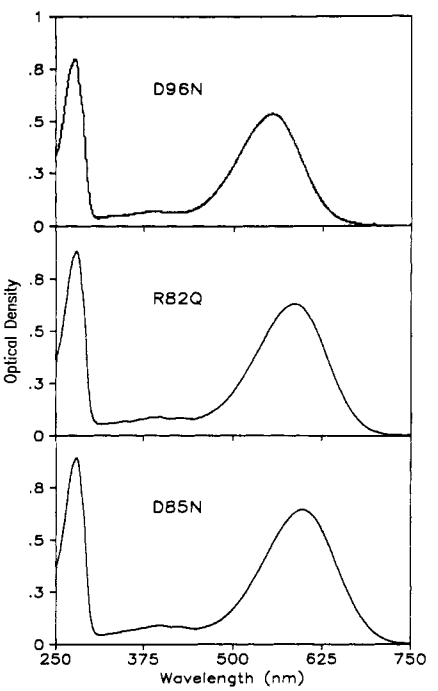

FIGURE 4: Absorption spectra of DA-purified monomers of e-BR from mutants in NG, pH 5.0. Absorbance maxima of D96N, R82Q, and D85N are 556, 585, and 596 nm, respectively.

amounts of induced cells, only D96N was recovered in amounts identical with e-BR (Table II). R82Q and D85N were recovered at 85% and 50% of the amount of e-BR, respectively. Relative to e-BO, purified D85N-, D96N-, and R82Q-substituted proteins had progressively larger values of $t_{1/2}$ (2.1, 4.6, and 170 min) consistent with an effect on protein–retinal stability, and progressively red-shifted absorption maxima consistent with their effects on the chromophore environment (Table I). D96N, R82Q, and D85N had progressive increases in $A_{280nm}/A_{\lambda_{max}}$ after HPSEC and hence progressive decreases in yield (Table II). After dye–ligand chromatography and exchange into NG, the purity based on comparison of the total protein measured by the Lowry method and the absorbance at λ_{max} and the optical purity of BR variants increased to ~100% with dark-adapted absorbance ratios ($A_{280nm}/A_{\lambda_{max}}$) of 1.5 (Figure 4, Table II). The absorbance maxima in NG of BR variants D85N and R82Q (Figure 4) were significantly blue-shifted from their values in CHAPSO (Figure 3, Table I).

Proton Pumping Activity. e-BR, w-BR, and d-BR have identical proton pumping characteristics (Figure 5A,B). The initial rate of proton pumping rises linearly as a function of light intensity (Figure 5A, upper lines). Thus, any proton leakage from the vesicles due to the lowering of internal pH does not affect initial rates through this range of light intensity. A value of 32 mW/cm^2 was chosen as standard for relating pH-dependent activity since the linearity decreases slightly at higher light intensities. The steady-state pumping rate rises at higher light intensity; however, its rate of increase pro-

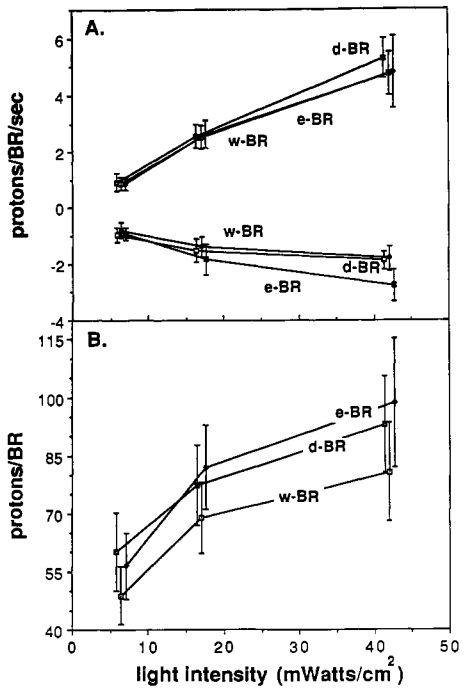

FIGURE 5: Light-induced proton pumping properties of e-BR, w-BR, and d-BR incorporated into soybean phospholipid vesicles. Proton pumping is plotted versus light intensity. (A) Upper lines (positive rates) correspond to initial rates of pH drop on illumination, before any pH gradient is generated across the vesicle membrane, and are linearly dependent on light. Lower lines (negative rates) correspond to the decay rates after light is extinguished and are driven by the pH gradient that was generated in the steady-state condition. (B) Steady-state pH change upon equilibration in light. The steady-state pumping rate reflects the net proton flux pumped (i.e., protons pumped in minus protons pumped out and leakage of protons out) into the vesicles. Error bars represent the standard deviations computed from 10–30 measurements at each point, taken from 4–8 different liposome preparations.

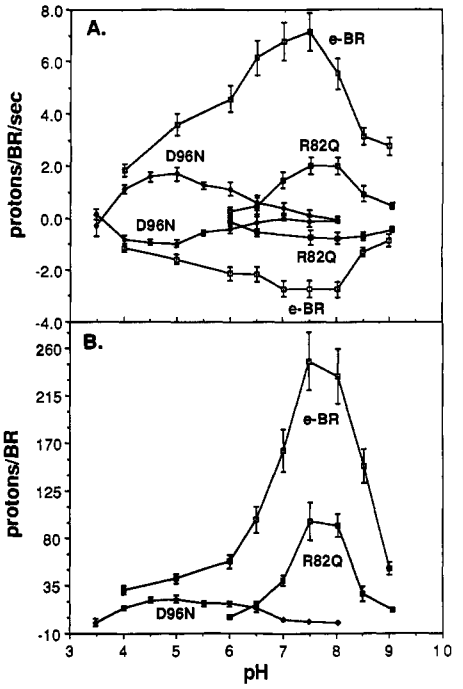

FIGURE 6: Light-induced proton pumping by e-BR, D96N, and R82Q versus external pH at 32 mW/cm². D85N had no pumping at any pH and was omitted for clarity. (A) Upper traces are initial rates; lower traces are decay rates after light is removed. (B) Steady-state pH change. Error bars represent the standard deviations computed from 5–12 measurements at each point, taken from 3 different liposome preparations.

gressively diminished by the pH gradient-induced leakage rate (Figure 5B). The decay rates (Figure 5A, lower lines) after the light is extinguished are about 50% of the initial pumping rates. Since leakage and net pumping rates are equal in the steady state, either the proton leakage rate drops by 50% in the absence of light or the light-driven outward pumping rate per BR molecule, from a lower internal pH (higher proton concentration) by the ~31 ± 4% molecules of BR facing outward, is greater than the inward pumping rate at steady state.

pH Dependence of Proton Pumping. The initial rate of proton pumping and the decay rate of e-BR from wild type and mutants are depicted in Figure 6A as a function of external pH. Steady-state rates show a generally similar pH dependence (Figure 6B). In our vesicle system, e-BR and w-BR (data not shown) have maximum activity at pH 7.5, and rates decrease with 50% of the initial rates at pH 8.5 and 5.5 (pH 7.0 for steady-state rates). The diminution of pumping observed at high and low pH is reversible by titration back to pH 7.5. Above pH 8.5, e-BR is unstable since light-dependent pumping rates progressively decreased with multiple exposures.

D85N had no detectable pumping at any pH, whereas R82Q had the same pH dependence as e-BR but demonstrated only 28% of the initial rate and 39% of the steady-state rate. D96N had a small but significant initial and steady-state pumping rate (24% and 9% of e-BR, respectively) with drastically altered pH dependence. D96N had maximal activity at pH 5.0 and diminished with 50% maximal values at pH 4.0 and 6.2. Ninety percent of the wild-type pH-dependent pumping profile activity of D96N was restored in the presence of 4 mM azide (data not shown).

Crystallization and Structure of e-BR. Initially, the reconstituted samples of e-BR in *H. halobium* lipids consisted of circular sheets and vesicles of various sizes. After 2 months, tubular vesicles containing an orthorhombic surface lattice of crystalline e-BR grew with dimensions averaging 0.8 × 0.2 μm (Figure 7). Low-dose images from uranyl formate stained tubular vesicles give optical diffraction to about 23-Å resolution. The lattices have orthorhombic symmetry, plane group *pgg*, with unit cell dimensions a = 127 Å and b = 67 Å. Following longer incubation, patches which contained lattices with trigonal *p3* symmetry that diffracted well, very similar to, and as well-ordered as those found in PM were obtained (Figure 8). The unit cell dimension was a = 64.2 ± 0.4 Å, calibrated by using the 2.04-Å [200] reflection from cubic gold crystals. At room temperature, diffraction to a resolution exceeding 3.7 Å is observed. In PM, the resolution limit is similar at room temperature but extends to 2.65 Å at −120 °C (Hayward & Stroud, 1981). The e-BR sheets should therefore permit difference mapping to 2.65 Å. The diffraction pattern is qualitatively similar to those from PM, indicating that the structure of e-BR matches that of wild-type PM quite closely, and suggesting that the N terminus is flexible in e-BR since the different length distribution at this end is not seen as a difference in the diffraction pattern that would be expected if these residues were ordered. Since the 2-D crystals are twinned, a quantitative comparison requires detwinning the relative contributions of each lattice from the observed intensities (Mitra & Stroud, 1990). Once this is accomplished, the diffraction patterns from e-BR will be compared to those of variants, to quantitate the differences in structure precisely.

Discussion

We have produced pure, functional wild-type and mutant forms of bacteriorhodopsin suitable for functional charac-

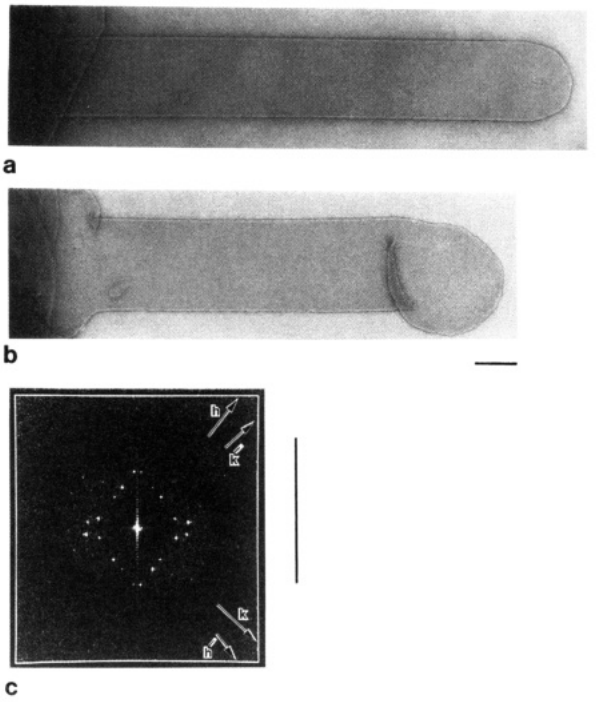

FIGURE 7: (A, B) Electron micrographs of uranyl formate stained tubular crystals of e-BR recorded under low-dose conditions at a magnification of 31500× [calibrated by using images of beef liver catalase (Unwin, 1975)] under an accelerating voltage of 80 kV. This figure was reproduced at 40% of its original size. Total dose was ~10 e/Å^2. The horizontal bar corresponds to 1000 Å. (C) A computed Fourier transform of a scanned image of a tubular crystal, such as that seen in (A, B), reveals diffraction from an ordered array. Indexing according to indices along the major reciprocal lattice directions is indicated by h, k and h', k'. The vertical bar represents the axial direction of the tube from which the transform was obtained.

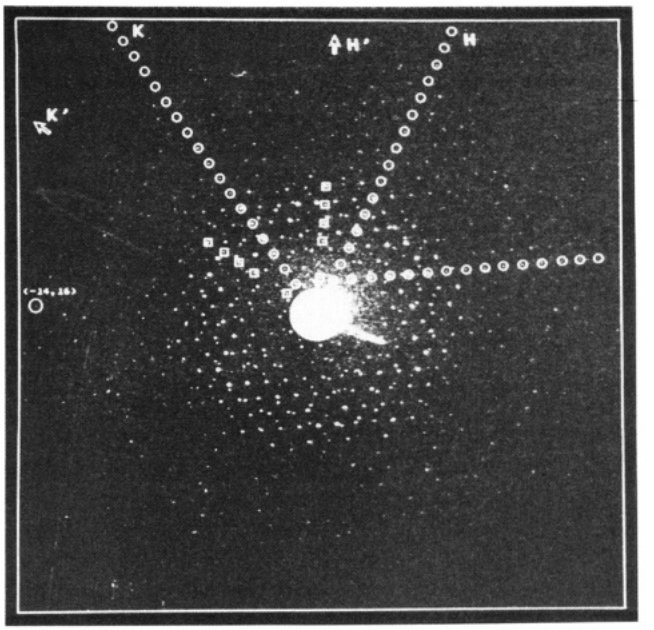

FIGURE 8: Low-dose electron diffraction recorded from glucose-sustained trigonal *p3* lattices formed after annealing shows a highly ordered pattern extending to beyond 3.7-Å resolution. The pattern is from two lattices oriented at an angle of 22° with respect to each other. The figure is for a digitized image of the diffraction pattern after removing most of the background contributed by radial inelastic scatter. The unit cell dimension is $a = 64.20 \pm 0.40$ Å determined by using the 2.04-Å [200] reflection from oriented gold crystal as a calibration standard. Reflections along the major reciprocal lattice directions H and K, and H' and K' corresponding to the two lattices, are surrounded by open circles and open squares, respectively. The reciprocal lattice defined by the directions H and K shows more intense reflections with the visible highest resolution reflection (−14, 16) corresponding to 3.68-Å resolution marked. Also encircled are an intense row of reflections corresponding to $H + K = 2$ ($H \geq 2$) for the stronger lattice. This figure was generated by using the program PRISM (Chen et al., 1990).

terization and high-resolution structural analysis by diffraction methods. Diffraction from e-BR lattices provides a sensitive assay of any conformational change produced by amino acid substitution, using difference Fourier density maps. This is an important factor in assessing effects of amino acid substitutions which produce a shift of the absorbance maximum, implying a change in the chromophore environment. Any discussion of electrostatic versus structural change also requires knowledge of the induced structural alteration.

In the preceding paper (Shand et al., 1991), we establish an *E. coli* expression system capable of producing 10–20-fold more BO than previously reported for BO expressed in *E. coli* (Karnik et al., 1987; Braiman et al., 1987). Our purification scheme for e-BO avoids use of a complex micelle containing DMPC, CHAPS, and SDS, and liposome environment such as the one containing soybean phospholipids, DMPC, CHAPS, SDS, and OG used previously (Braiman et al., 1987). The overall yield of e-BR produced by our scheme is ~60% of BO present in the fractions taken from the first column (Figure 1A, and inset). The procedure produces large amounts of pure e-BR from wild type or mutants, in a single detergent, with no contamination by e-BO or other proteins. At pH 5.0, an $A_{280nm}/A_{\lambda_{max}}$ ratio of 1.5 corresponds to ~100% pure monomeric BR (Table II). This purity may be of advantage for biophysical studies. Our approach was based on the notion that membrane proteins purified and folded in appropriate detergents provide better prospects for crystallization and functional analyses. e-BR (or w-BR) prepared by column chromatography using detergents can be crystallized to form two-dimensional trigonal lattices identical with the well-characterized BR lattices, and tubular crystals with a previously undescribed orthorhombic lattice. The degree of order in the crystals is represented as the highest resolution attainable in the diffraction patterns, and was found by electron diffraction to be almost the same resolution (~3.7 Å at room temperature) as for PM or reconstituted sheets of BR under the same conditions.

Examination of purified e-BO revealed that minor post-translational processing of the e-BO leader sequence occurred in *E. coli* [Figure 2B and Shand et al. (1991)], which resulted in an N-terminal heterogeneity reminiscent of that observed previously in w-BR (Wolfer et al., 1988; Miercke et al., 1989a). Nevertheless, the presence of the extra N-terminal residues with minor truncations did not affect folding kinetics, absorption spectra, or proton pumping. The e-BR and M_{412} chromophore geometry and environment (Lin et al., 1990) and e-BR photocycle kinetics (D. Kliger, personal communication) are also identical with those for w-BR. Therefore, our expressed protein is functionally identical. From the structural standpoint, 2-D crystals that grow from material containing the three e-BR species have closely similar unit cell dimensions to those that are formed from w-BR which has greater N-terminal heterogeneity. e-BR also crystallizes with a second, orthorhombic lattice (a = 127 Å, b = 67 Å) not previously observed for w-BR. The orthorhombic lattice for w-BR observed earlier by Michel et al. (1980) by reconstitution in the presence of cationic detergents has dimensions a = 57.6 Å and b = 73.5 Å.

One parameter for characterizing the functional roles of amino acids in BR is light-induced proton pumping. In terms of proton pumping versus light intensity and external pH, e-BR

behaves essentially identically with w-BR. The initial rates of pumping upon illumination where there is no pH gradient across the vesicle membrane were linearly proportional to light intensity (Figure 5A) and provide a precise, and probably our best, measure of functional activity since the membrane potential and proton gradient are minimal. The slight fall off in the steady-state rate at higher light intensity (Figure 5B) is consistent with further excitation of photointermediates. The interpretation of steady-state activities is complicated by the higher internal proton concentration in the vesicles achieved by net inward pumping. The molecules oriented to pump outward (~30%) are pumping from a proton-rich environment and so at steady state may have a higher pumping rate than the remaining molecules (~70%) which face inward. The decay rate determined after the light is turned off assesses the pH gradient dependent leak rate. While initial rates are probably the most reliable, the steady-state and decay values serve to confirm the reproducibility of vesicle preparations. pH-dependent initial, steady-state, and decay rates are highly reproducible and provide an estimate of functional efficiency. Thus, these measurements can reliably be used to calibrate the effects of site-directed mutations.

The pH optimum for e-BR is at pH 7.5 for both initial and steady-state pumping, and it is diminished by a factor of ~2 in the initial rate or ~5 in the steady-state rate at pH 5.5, and by a factor of ~2 at pH 8.5. In contrast to our vesicles with BR monomers, *H. halobium* cell envelopes containing PM have a constant pumping rate between pH 4.0 and pH 6.5, diminishing due to the acid transition at pH ~3.5, and diminishing at high pH, above pH 7.0–9.0, where the lifetime of the N intermediate increases exponentially with pH (Kouyama & Kouyama, 1989). The $N_{550} \rightarrow BR_{568}$ transition depends on the protonation of Asp-96, and the lowered concentration of protons at high pH accounts for the drop in activity at high pH (Ames & Mathies, 1990).

In contrast to our results, the pH dependence of the initial rate recorded over the narrower range pH 7.5–5.5 in a complex vesicle environment showed the opposite trend, with no change or a slight increase of pumping by e-BR at pH 5.5 (Stern & Khorana, 1989). The differences in the observed pH-dependent profile for e-BR cannot simply be explained by different vesicle composition since the low-pH limb of R82Q activity is similar in both studies; thus, some interaction between lipid and chromophore environment must be in evidence. The pH profile in vesicles (Figure 6) is sharper than the profile for cell envelope vesicles. Similarly conflicting results between cell envelope vesicles and proteoliposomes were observed for HR, where the activity in cell envelopes was pH independent while purified HR reconstituted into liposomes was pH dependent with maximum light-induced chloride pumping activity at pH 6.0 (Duschl et al., 1988). Thus, the unusual sulfurylated lipids (Kates et al., 1982) and/or the asymmetry of lipid charge found in PM (Fisher et al., 1978) seem to reduce pH dependence, suggesting that titration of the lipids is in part responsible for the pH dependence observed in soybean phospholipids.

D85N, D96N, and R82Q, when expressed, purified, and functionally characterized in the same manner as for e-BO, have altered properties similar to those reported previously. These variants each have a replacement of one charged residue in helix C of BR by a neutral side chain of similar size. The pH dependence of activity was measured between pH 4.0 and pH 9.0 (Figure 6A,B). D85N has no pumping at any pH. Proton pumping by D96N and R82Q when reconstituted into soybean phospholipid vesicles can be compared with the pH dependence of pumping recently reported for e-BR and D96N (Holz et al., 1989), and for R82Q (Stern & Khorana, 1989), even though significantly different conditions were used, and over a narrower pH range from 5.5 to 7.5. The pH dependence of R82Q between pH 5.5 and 7.5 (Stern & Khorana, 1989) and that of D96N (Holz et al., 1989) are qualitatively similar to the respective portions of our pH profiles.

The pH-dependent losses of activity shown in Figure 6 are completely reversible as the pH is restored. pH does not seem to affect λ_{max}, suggesting that alteration in pumping is due to electrogenic rather than structural changes. pH-dependent absorption spectra can be measured directly in vesicles using an integration sphere, instead of indirectly by use of detergent-solubilized vesicles as described here and by Subramaniam et al. (1990). The $N_{550} \rightarrow O_{640}$ transition has a marked pH dependence, indicating that proton uptake occurs during N_{550} decay (Ames & Mathies, 1990). Thus, N decay may depend on $[H^+]$ for uptake, possibly due to protonation of Asp-96 which has a pK_a of ~6.5 (Figure 6A). The decrease in activity at low pH may be due to protonation of other functionally important residues which are required to be charged.

Aspartic Acid-85. The D85N mutation affects the retinylation rate and extent, shifts the absorption maximum from purple to blue (548 to ~590 nm; Table II), and abolishes pumping by preventing formation of the M_{412} intermediate (Stern et al., 1989). The absence of any proton pumping by D85N suggests that the charge on Asp-85 is required for function. Our D85N pumping results are similar to previous observations (Mogi et al., 1988). Asp-85 is unprotonated in the ground state, with a pK_a of ~2.5 (Rothschild et al., 1981), and becomes protonated in the L → M transition (Braiman et al., 1988; Gerwert et al., 1989). Thus, Asp-85 probably serves as a counterion to the Schiff base at Lys-216 in the ground state, and as the direct proton acceptor during the $L_{550} \rightarrow M_{412}$ transition (see Figure 9). The environment is maintained by the charge on Arg-82 and Asp-212, and substitutions of these residues may moderate the proton affinity of Asp-85 (Otto et al., 1990). The monomer structure is seemingly less constrained in D85N (and R82Q) since the absorption maximum is dependent on the detergent environment (compare Figures 3 and 4, Table II).

The location of charge on Asp-85 seems to be critical, since D85E decreases the time required for retinylation with little change in the extent (Mogi et al., 1988). The retinal pocket seems to be more accessible in D85E since retinal can be cleaved from Lys-216 by treatment with hydroxylamine in the dark (Soppa et al., 1989). The substitution of a side chain one methylene group longer reduces pumping by 70% (Mogi et al., 1988), produces a pH-dependent proton pumping rate which correlates with a change in the purple to blue transition (Soppa et al., 1989; Subramaniam et al., 1990), and accelerates the rise of M_{412} and the positive component of the light-induced charge displacement current (Butt et al., 1989). Together, these observations indicate that Asp-85, with its unusual acidity (pK_a of ~2.5; Rothschild et al., 1981), serves as the counterion to the Schiff-base and is the direct proton acceptor during the photocycle. The charges on Arg-82 and Asp-212 appear to moderate the proton affinity of the proton acceptor Asp-85 (Braiman et al., 1988; Otto et al., 1990) in the immediate vicinity of the Schiff base.

Aspartic Acid-96. Replacement of Asp-96 with asparagine greatly decreases the proton pumping efficiency (Soppa & Oesterhelt, 1989; Mogi et al., 1988) as seen in Figure 6. Diminished pumping is due to effects seen at two steps in the

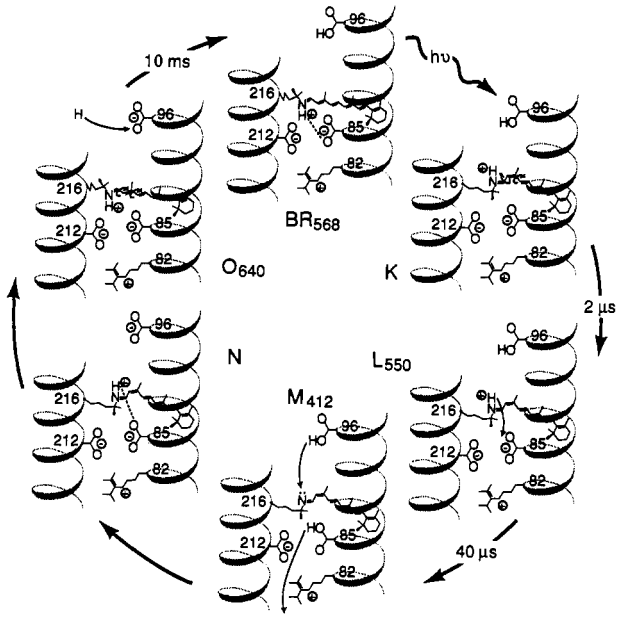

FIGURE 9: Representation of a possible mechanism for involvement of residues Asp-85, Asp-96, and Arg-82 in the photoreaction cycle and in proton translocation. Helices G and C are depicted along with pertinent residues. Retinal is attached to Lys-216 by a Schiff base. The cycle starts with isomerization about the C13=C14 bond of retinal. The Schiff base is deprotonated in the L → M transition and reprotonated in the M → N transition with reisomerization at N → O. Changes in structure of the chromophore in the different intermediates are indicated, and the cis–trans isomerization is indicated alongside the postulated charged state of pertinent residues including those that were substituted.

latter part of the photocycle, both of which become pH sensitive. First, M_{412} decay and the positive photovoltage decay are slowed, corresponding to slowed reprotonation of the Schiff base (Holz et al., 1989; Otto et al., 1989, 1990; Butt et al., 1989; Stern et al., 1989). Second, there is a slowed charge displacement and reduced conductivity which correspond to slowed uptake of protons by the protein at Asp-96 (Marinetti et al., 1989; Holtz et al., 1989). However, the stoichiometry of protons pumped per photocycle (H^+/M_{412}) remains the same as for e-BR (Holz et al., 1989), suggesting that Asp-96 lies in the reprotonation pathway. Asp-96 is initially protonated in the photocycle and remains so until decay of the M intermediate (Gerwert et al., 1989; Braiman et al., 1988) (see Figure 9). Together this shows that Asp-96 has a role as proton donor during the reprotonation of the Schiff base from the cytoplasmic surface. However, it is not indispensable since reprotonation of the Schiff base occurs at low pH (~5), about 20% as efficiently in e-BR (Figure 5). Thus, some other intermediate group, or water, may be involved between Asp-96 and the Schiff base. Protons may be directly restored to the Schiff base at low pH as suggested by Holz et al. (1989). Yet as the pH is decreased below pH 4.0, activity of D96N is diminished (Figure 6A,B), again suggesting that one or more unprotonated residue of pK_a ~4.0 is important for function, or for maintaining structure. By random mutagenesis in *H. halobium* sp. GRB, Soppa and Oesterhelt (1989) found mutations of altered phenotype; D96N and D96G had a slowed photocycle but with the same spectral characteristics, indicating that Asp-96 lies in the reprotonation pathway but is not close enough to the Schiff base to alter its electronic structure. The spatial location of the Asp-96 carboxyl group is not crucial since D96E, in which pH-dependent proton uptake is slowed, has a normal quantum yield (Marinetti et al., 1989), is 100% active (Mogi et al., 1988), has essentially no change in photovoltage, and has little perturbation in the M decay (Holz et al., 1989; Otto et al., 1990). Resonance Raman spectra show that the D96N chromophore in BR_{570}, where it is protonated, and in M_{412} species, where it is unprotonated, are identical in wild-type BR (Lin et al., 1991). This also shows that Asp-96 is not close to the chromophore. Thus, Asp-96 at the cytoplasmic side of helix C, some 15 Å from Asp-85, is too far away to directly reprotonate the Schiff base, implying that other functional groups must be involved. Threonine-89 on the same side of helix C or possibly bound water are candidates.

The pumping of D96N is almost completely restored by 4 mM azide (see Results) or other anions, consistent with a role for N_3^- anion in replacing the carboxylate of Asp-96 in the protein structure and in proton transfer (Tittor et al., 1989). This anion site may be related to outward pumping of chloride anion by the homologous HR protein, in which Asp-96 on the cytoplasmic side of the Schiff base is replaced by alanine. In HR, the Cl^- site may be analogous to the N_3^- site in D96N. The modulation of Cl^- binding at this and at another site on the other side of the chromophore during the photocycle is a model for pumping of Cl^- in HR.

As observed here and by Mogi et al. (1988), D96N does not appear to induce structural changes since there is little effect on retinylation rate and extent and DA/LA absorption properties. Holz et al. (1989) state that the hexagonal lattice of D96N was identical with PM, suggesting that D96N may not affect structure much more than expected in the region around D96. Therefore, Asp-96 exerts little electrostatic effect on the Schiff base and acts primarily in proton transfer.

Arginine-82. R82Q has 40% of the pumping rate of e-BR at pH 7.5 (Figure 6A,B) and has a significant effect on the absorbance maximum of the chromophore (Table I). Thus, Arg-82 is not absolutely required for proton pumping as is Asp-85. Initial and steady-state pumping rates by R82Q show a pH dependence characterized by an apparent pK_a of ~6.7. This parallels a change in the chromophore absorbance that is red-shifted at lower pH, below pH 7.0. Therefore, the charge on Arg-82 affects the pK_a of the Schiff base (Otto et al., 1990). In addition, Arg-82 might help to maintain a low pK_a for Asp-85, making it a better proton acceptor. However, the rise and decay of the M intermediate, where proton transfer to Asp-85 and reprotonation of the Schiff base are involved, are both faster in the overall less efficient R82Q. This is consistent with a higher proton affinity of Asp-85 as expected for a raised pK_a. The slowed step is proton release from Asp-85 (Otto et al., 1990). After substitution of each of the seven arginines with glutamine, R82Q and R227Q were the only ones to affect the function of BR (Stern & Khorana, 1989). The side chain of Asp-85 is close to the side chain of Arg-82 since they lie on the same side of helix C with α-carbon atoms ~5.5 Å apart.

Purple to Blue Transition in BR. The purple membrane becomes blue, either when the pH is lowered, reducing the charge on certain carboxylic acid side chains, or upon removal of divalent cations whose role may be to maintain either the charged state of carboxylic acids (Chang et al., 1985) or the membrane potential (Kimura et al., 1984). Thus, the purple to blue transition is a sensitive assay of the electrostatic environment of the chromophore. Substitution of Arg-82, Asp-85, or Asp-212 results in an altered pK_a of the purple to blue transition of the chromophore (Mogi et al., 1988) and affects proton release from BR (Otto et al., 1990). The blue membrane (BR_{605}) does not pump protons (Drachev et al., 1978; Mowery et al., 1979; Fischer & Oesterhelt, 1979). However, the K_{610} and O_{640} intermediates in the photoreaction

cycle are also blue. This indicates that there is probably a correspondence between the charge-induced structure change that is seen in the stable blue species and the transient intermediates. D85N remains blue at all pHs. Action spectra, relating pumping to the wavelength of actinic light, associate the inactivity of D85N with the loss of charge on Asp-85, as the counterion for the Schiff base (Subramaniam et al., 1990). The pK_a of the Schiff base is normally ~13 but is reduced to ~7.4 in D85N where it is no longer stabilized by the charge on Asp-85 (Otto et al., 1990). Substitution of a neutral asparagine in D212N prevents the transition to blue which led Subramaniam et al. (1990) to propose that Asp-85 is the counterion to the Schiff base in the purple species and D212 is the counterion for the Schiff base in the blue membrane. Whether the purple to blue transition is due to titration of a carboxyl group near the chromophore as suggested by Fischer and Oesterhelt (1979), to a change in surface potential (Szundi & Stoeckenius, 1988, 1989), or to a change in the strength of hydrogen bonding to the Schiff base remains in question. However, there are distinct cation binding sites on the purple membrane as seen by X-ray diffraction (Katre et al., 1986) and by electron microscopy (Mitra & Stroud, 1990). In addition, Fourier transform infrared spectroscopy identifies specific changes in the protein structure, and in carboxyl groups that may be involved in cation binding (Dunach et al., 1989). Thus, structural or electronic changes which occur in the purple–blue transition reflect changes that are brought about by mutations, which emphasizes the need for knowledge of the structural changes that occur in the vicinity of the chromophore.

Comparison with a Model of BR. The roles for Asp-85, Asp-96, and Arg-82 deduced from the pH dependence of proton pumping are consistent with their positions in helix C relative to the Schiff base at Lys-216 in helix G (see Figure 9). However, Asp-96 is too far from the Schiff base to be directly involved in reprotonating the Schiff base, and the question of what intermediate proton-transfer mechanisms are possible remains.

References

Alshuth, T., Stockburger, M., Hegemann, P., & Oesterhelt, D. (1985) *FEBS Lett. 179*, 55–59.

Ames, J. B., & Mathies, R. A. (1990) *Biochemistry* (submitted for publication).

Baldwin, J. M., Henderson, R., Beckman, E., & Zemlin, F. (1988) *J. Mol. Biol. 202*, 585–591.

Bayley, H., Huang, K.-S., Radhakrishnan, R., Ross, A. H., Takagaki, Y., & Khorana, H. G. (1981) *Proc. Natl. Acad. Sci. U.S.A. 78*, 2225–2229.

Blanck, A., & Oesterhelt, D. (1987) *EMBO J. 6*, 265–273.

Braiman, M. S., Stern, L. J., Chao, B. H., & Khorana, H. G. (1987) *J. Biol. Chem. 262*, 9271–9276.

Braiman, M. S., Mogi, T., Marti, T., Stern, L. J., Khorana, H. G., & Rothschild, K. J. (1988) *Biochemistry 27*, 8516–8520.

Butt, H. J., Fendler, K., Bamburg, E., Tittor, J., & Oesterhelt, D. (1989) *EMBO J. 8*, 1657–1663.

Chang, C. H. J.-G., Chen, R., Govindjee, R., & Ebrey, T. (1985) *Proc. Natl. Acad. Sci. U.S.A. 82*, 396–400.

Chen, H., Sedat, J., & Agard, D. (1990) in *Handbook of Biological Confocal Microscopy* (Pawley, J., Ed.) pp 141–150, Plenum Publishing Corp., New York.

Drachev, L. A., Kaulen, A. D., & Skulachev, V. P. (1978) *FEBS Lett. 87*, 161–167.

Dunach, M., Padros, E., Muga, A., & Arrondo, J. L. (1989) *Biochemistry 28*, 8940–8945.

Duschl, A., McCloskey, M. A., & Lanyi, J. K. (1988) *J. Biol. Chem. 163*, 17016–17022.

Earnest, T. N., Roepe, P., Braiman, M. S., Gillespie, J., & Rothschild, K. J. (1986) *Biochemistry 25*, 7793–7798.

Fischer, U., & Oesterhelt, D. (1979) *Biophys. J. 28*, 211–230.

Fisher, K. A., Yanagimoto, K., & Stoeckenius, W. (1978) *J. Cell Biol. 77*, 611–621.

Fodor, S. P. A., Ames, J. B., Gebhard, R., van den Berg, Stoeckenius, W., Lugtenberg, J., & Mathies, R. A. (1988) *Biochemistry 27*, 7097–7101.

Gerwert, K., Hess, B., Soppa, J., & Oesterhelt, D. (1989) *Proc. Natl. Acad. Sci. U.S.A. 86*, 4943–4947.

Hayward, S. B., & Glaeser, R. M. (1980) *Ultramicroscopy 5*, 3–8.

Hayward, S. B., & Stroud, R. M. (1981) *J. Mol. Biol. 151*, 491–517.

Henderson, R., Baldwin, J. M., Downing, K. H., Lepault, J., & Zemlin, F. (1986) *Ultramicroscopy 19*, 139–150.

Henderson, R., Baldwin, J. M., Ceska, T. A., Zemlin, F., Beckmann, E., & Downing, K. H. (1990) *J. Mol. Biol. 213*, 899–929.

Heyn, M. P., Cherry, R. J., & Muller, U. (1977) *J. Mol. Biol. 117*, 607–620.

Hofrichter, J., Henry, E. R. T., & Lozier, R. H. (1989) *Biophys. J. 56*, 693–706.

Holz, M., Drachev, L. A., Mogi, T., Otto, H., Kaulen, A. D., Heyn, M. P., Skulachev, V. P., & Khorana, H. G. (1989) *Proc. Natl. Acad. Sci. U.S.A. 86*, 2167–2171.

Karnik, S. S., Nassal, M., Doi, T., Jay, E., Sgaramella, V., & Khorana, H. G. (1987) *J. Biol. Chem. 262*, 9255–9263.

Kates, M., Kushawa, S. C., & Sprott, G. D. (1982) *Methods Enzymol. 88*, 98–111.

Katre, N. V., Wolber, P. K., Stoeckenius, W., & Stroud, R. M. (1981) *Proc. Natl. Acad. Sci. U.S.A. 78*, 4068–4072.

Katre, N. V., Kimura, Y., & Stroud, R. M. (1986) *Biophys. J. 50*, 277–284.

Khorana, H. G. (1988) *J. Biol. Chem. 263*, 7439–7442.

Kimura, Y., Ikegami, A., & Stoeckenius, W. (1984) *Photochem. Photobiol. 40*, 641–646.

Kouyama, T., & Nasuda-Kouyama, A. (1989) *Biochemistry 28*, 5963–5970.

Kouyama, T., Nasuda-Kouyama, A., Ikegami, A., Mathew, M. K., & Stoeckenius, W. (1988) *Biochemistry 27*, 5855–5863.

Lin, S. W., & Mathies, R. A. (1989) *Biophys. J. 56*, 653–660.

Lin, S. W., Fodor, S. P. A., Miercke, L. J. W., Shand, R. F., Betlach, M. C., Stroud, R. M., & Mathies, R. A. (1991) *Photochem. Photobiol. 53*, 341–346.

Lowry, O. H., Rosebrough, N. J., Farr, A. L., & Randall, R. J. (1951) *J. Biol. Chem. 193*, 265–275.

Lozier, R. H., Bogomolni, R. A., & Stoeckenius, W. (1975) *Biophys. J. 15*, 955–962.

Lozier, R. H., Niederberger, W., Bogomolni, R. A., Hwang, S., & Stoeckenius, W. (1976) *Biochim. Biophys. Acta 440*, 545–546.

Marinetti, T., Subramaniam, S., Mogi, T., Marti, T., & Khorana, H. G. (1989) *Proc. Natl. Acad. Sci. U.S.A. 86*, 529–533.

Mathies, R. A., Brito-Cruz, C. H., Pollard, W. T., & Shank, C. V. (1988) *Science 240*, 777–779.

Michel, H., Oesterhelt, D., & Henderson, R. (1980) *Proc. Natl. Acad. Sci. U.S.A. 77*, 338–342.

Miercke, L. J. W., Ross, P. E., Stroud, R. M., & Dratz, E. A. (1989a) *J. Biol. Chem. 264*, 7531–7535.

Miercke, L. J. W., Stroud, R. M., & Dratz, E. A. (1989b) *J. Chromatogr. 483*, 331-340.
Milder, S. J., Thorgeirsson, T. E., Miercke, L. J. W., Stroud, R. M., & Kliger, D. S. (1991) *Biochemistry 30*, 1751-1761.
Mitra, A. K., & Stroud, R. M. (1990) *Biophys. J. 57*, 301-311.
Mogi, T., Stern, L. J., Hackett, N. R., & Khorana, H. G. (1988) *Proc. Natl. Acad. Sci. U.S.A. 85*, 4148-4152.
Mowery, P. C., Lozier, R. H., Chae, Q., Tseng, Y.-W., Taylor, M., & Stoeckenius, W. (1979) *Biochemistry 18*, 4100-4107.
Oesterhelt, D., & Tittor, J. (1989) *Trends Biochem. Sci. (Pers. Ed.) 14*, 57-61.
Otto, H., Marti, T., Holz, M., Mogi, T., Lindau, M., Khorana, H. G., & Heyn, M. P. (1989) *Proc. Natl. Acad. Sci. U.S.A. 86*, 9228-9232.
Otto, H., Marti, T., Holz, M., Mogi, T., Stern, L. J., Engel, F., Khorana, H. G., & Heyn, M. P. (1990) *Proc. Natl. Acad. Sci. U.S.A. 87*, 1018-1022.
Rothschild, K. J., Zagaeske, M., & Cantore, W. A. (1981) *Biochem. Biophys. Res. Commun. 103*, 483-489.
Rothschild, K. J., Argade, P. V., Earnest, T. N., Huang, K.-S., London, E., Liao, M.-J., Bayley, H., Khorana, H. G., & Herzfeld, J. (1982) *J. Biol. Chem. 257*, 8592-8595.
Shand, R. F., Miercke, L. J. W., Mitra, A. K., Fong, S. K., Stroud, R. M., & Betlach, M. C. (1991) *Biochemistry* (preceding paper in this issue).
Smith, S. O., Pardoen, J. A., Mulder, P. P., Curry, B., Lugtenburg, J., & Mathies, R. (1983) *Biochemistry 22*, 6141-6148.
Smith, S. O., Marvin, M. J., Bogomolni, R. A., & Mathies, R. (1984) *J. Biol. Chem. 259*, 12326-12329.
Soppa, J., & Oesterhelt, D. (1989) *J. Biol. Chem. 264*, 13043-13048.
Soppa, J., Otomo, J., Straub, J., Tittor, J., Meessen, S., & Oesterhelt, D. (1989) *J. Biol. Chem. 264*, 13049-13056.
Stern, L. J., & Khorana, H. G. (1989) *J. Biol. Chem. 264*, 14202-14208.
Stern, L. J., Ahl, P. L., Marti, T., Mogi, T., Dunach, M., Berkowitz, S., Rothschild, K. J., & Khorana, H. G. (1989) *Biochemistry 28*, 10035-10042.
Subramaniam, S., Marti, T., & Khorana, H. G. (1990) *Proc. Natl. Acad. Sci. U.S.A. 87*, 1013-1017.
Szundi, I., & Stoeckenius, W. (1988) *Biophys. J. 54*, 227-232.
Szundi, I., & Stoeckenius, W. (1989) *Biophys. J. 56*, 369-383.
Tittor, J., Soell, C., Oesterhelt, D., Butt, H. J., & Bamberg, E. (1989) *EMBO J. 8*, 1657-1663.
Unwin, P. N. T. (1975) *J. Mol. Biol. 98*, 235-242.
Williams, R. (1981) *J. Mol. Biol. 150*, 399-408.
Wolfer, U., Dencher, N. A., Buldt, G., & Wrede, P. (1988) *Eur. J. Biochem. 174*, 51-57.

A Major Proportion of N-Glycoproteins Are Transiently Glucosylated in the Endoplasmic Reticulum†

Sandra Gañán, Juan J. Cazzulo, and Armando J. Parodi*
Instituto de Investigaciones Bioquímicas, "Fundación Campomar", Antonio Machado 151, 1405 Buenos Aires, Argentina
Received October 2, 1990; Revised Manuscript Received December 5, 1990

ABSTRACT: N-Linked, high-mannose-type oligosaccharides lacking glucose residues may be transiently glucosylated directly from UDP-Glc in the endoplasmic reticulum of mammalian, plant, fungal, and protozoan cells. The products formed have been identified as N-linked $Glc_1Man_{5-9}GlcNAc_2$ and glucosidase II is apparently the enzyme responsible for the in vivo deglucosylation of the compounds. As newly glucosylated glycoproteins are immediately deglucosylated, it is unknown whether transient glucosylation involves all or nearly all N-linked glycoproteins or if, on the contrary, it only affects a minor proportion of them. In order to evaluate the molar proportion of N-linked oligosaccharides that are glucosylated, cells of the trypanosomatid protozoan *Trypanosoma cruzi* (a parasite transferring $Man_9GlcNAc_2$ in protein N-glycosylation) were grown in the presence of [^{14}C]glucose and concentrations of the glucosidase II inhibitors deoxynojirimycin and castanospermine that were more than 1000-fold higher than those required to produce a 50% inhibition of the *T. cruzi* enzyme. About 52-53% of total N-linked oligosaccharides appeared to have glucose residues. The compounds were identified as $Glc_1Man_{7-9}GlcNAc_2$. The same percentage was obtained when cells were pulsed-chased with [^{14}C]glucose in the presence of deoxynojirimycin for 60 min. No evidence for the presence of an endomannosidase yielding GlcMan from the glucosylated compounds was obtained. As the average number of N-linked oligosaccharides per molecule in glycoproteins is higher than one, these results indicate that more than 52-53% of total glycoproteins are glucosylated and that transient glucosylation is a major event in the normal processing of glycoproteins.

N-Glycosylation is initiated in most eukaryotes by the transfer of $Glc_3Man_9GlcNAc_2$ from a dolichol-P-P derivative to asparagine residues in polypeptide chains (Kornfeld & Kornfeld, 1985). This reaction, which occurs in the lumen of the rough endoplasmic reticulum, is immediately followed by the removal of the three glucose units from the protein-linked oligosaccharides. Two specific glucosidases are involved in the initial steps of oligosaccharide processing: glucosidase I, which cleaves the more external $\alpha(1,2)$-linked unit, and glucosidase II, which removes the remaining $\alpha(1,3)$-linked glucose residues. Two specific $\alpha(1,2)$-mannosidases located, as are both glucosidases, in the lumen of the endoplasmic

†This work was supported by grants from the National Research Council (Argentina), from the University of Buenos Aires, and from the United Nations Development Program/World Bank/World Health Organization Special Program for Research and Training in Tropical Diseases.
*Author to whom correspondence should be addressed.

0006-2960/91/0430-3098$02.50/0